Final Technical Report

Submitted to the
U.S. GEOLOGICAL SURVEY

By
CALIFORNIA INSTITUTE OF TECHNOLOGY

Grant No.:	Award No. G13AP00037
Principal Investigator:	Dr. Jean-Philippe Avouac California Institute of Technology 1200 E. California Blvd. MC 100-23 Pasadena, CA 91125 (626) 395-4239 Email: avouac@gps.caltech.edu
Project Title:	Measurements of surface ruptures produced by continental earthquakes from optical imagery and LiDAR
Effective Date of Contract:	June 2013 – June 2014
Date:	15 September 2014

ABSTRACT
Surface deformation produced by large continental earthquakes can be measured from correlation of optical satellite and aerial images. The technique provides information about the location and the motion of surface ruptures, for both strike-parallel and strike-perpendicular components of the surface slip. This information can be produced early on after an earthquake and can be used to constrain source models. It also provides a way to characterize surface ruptures of past earthquakes and revisit the empirical laws relating to earthquake magnitude, rupture length, mean and peak slip, which are commonly used in paleoseismology.
The technical advances which have enabled the technique have been implemented in the COSI-Corr software package. This proposal seeks support for application of the technique to upcoming earthquakes; the construction of a database to disseminate the results obtained on past earthquakes, and to enhance the technique so as to facilitate rapid application and extension to the use of LiDAR data.

RESULTS
While the amount of remote sensing data is rapidly increasing, methods to exploit them and provide objective information about the impact of environmental changes and natural disasters are lagging behind. Under this proposal, we developed a rigorous and versatile framework to measure 3D changes at the Earth's surface.

The tracking of 3D surfaces

Time series of DEMs extracted from stereogrammetry or LiDAR have been used in a number of studies to monitor changes over time due to a variety of processes, e.g., lava flow [*Favalli et al.*, 2010], glacier thinning [*Abermann et al.*, 2010; *Gardelle et al.*, 2012], coastal erosion [*Mitasova et al.*, 2009; *White and Wang*, 2003; *Woolard and Colby*, 2002]. In these studies, changes of elevation over time were determined from DEM differences. Provided that the DEM are perfectly registered and sampled on the same grid, this approach indeed readily quantifies erosion and deposition processes. In situations where a horizontal displacement is also involved (due to ice flow, landsliding, or co-seismic deformation for example), DEM differentiation yields an information about horizontal displacement as well as changes of the affected topography. For instance, let us consider that a point at location x is displaced by d_z vertically and by d_x horizontally. Let e be the change of elevation at that point due to erosion or sedimentation. Then, the elevation after the displacement h_2 and the initial elevation are linked by:

$$h_2(x) = h_1(x+d_x(x)) + d_z(x+d_x(x)) - e(x+d_x(x)), \qquad (1)$$

This equation can also be expressed as:

$$h_2(x-d_x) = h_1(x) + d_z(x) - e(x) \quad (2)$$

Then, using a first order approximation, we can linearize equation (1). The elevation difference depends on the local topographic gradient according to:

$$h_2(x) - h_1(x) \approx h_1'(x).\, d_x(x) + d_z(x+d_x(x)) - e(x+d_x(x)), \qquad (3)$$

where $h_1'(x)$ is the derivative of h_1 along Ox-plane at ground location x.
As the ground structures have moved horizontally, they are not physically aligned anymore in the DEM, and their morphologic evolution cannot be recovered by simply differentiating the DEM. In the case where topographic changes due to erosion and sedimentation can be neglected, $e(x)=0$, it would be more appropriate to determine the 3D displacement field from matching the two surfaces in three dimensions.

Examples of application to the El-Mayor Cucapah Earthquake, April 2010

In the wake of the El Mayor-Cucapah earthquake of April 4, 2010, we have collaborated with the USGS and JPL to analyze ground deformations. The first rupture map was obtained from correlating pre and post-earthquake SPOT images. These results revealed a prominent fault trace running through the Sierra Cucapah that the aerial survey carried on the day after the earthquake had mostly missed due to its unexpected location within the core of the Sierra (USGS - Ken Hudnut, personal communications). These results were posted on the UNAVCO web site (http://supersites.unavco.org/baja.php#Sun3), as well as the subsequent refined measurements (figure 1). These measurements have been combined with measurements obtained from correlating SAR amplitude images following a similar procedure to the one used to correlate the optical images. These measurements reveal a continuous fault trace of about 120 km with an average surface slip of about 2m. We have next determined a detailed earthquake source model using this information together with inSAR results (collaboration with Eric Fielding at JPL) and teleseismic waveforms modeling following the same approach as in some of our previous studies [e.g.,*Wei et al.*, 2011]. This study demonstrates the interest of image matching to early analysis of large earthquakes.

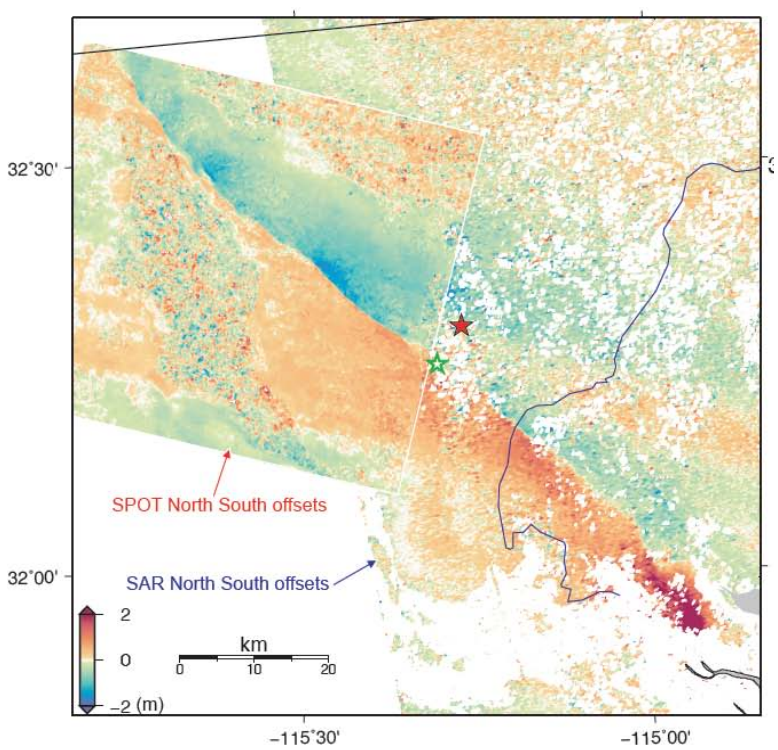

Figure 1. Composition image showing N-S surface displacements (positive northward) induced by the El Mayor-Cucapah earthquake obtained from correlating SPOT and SAR amplitude images. The star indicates the location of the epicenter.

The El-Mayor Cucapah earthquake is the first event for which pre and post-earthquake LiDAR data is available. Analysis of pre- and post-earthquake topographic data provides an opportunity to deliver the full 3D displacement field of the ground's surface. However, as explained previously, direct differencing of a pre- and post-earthquake digital topography model

(DEM) generally leads to biased estimation of the vertical component of the deformation, especially if the earthquake also produced significant horizontal motion. To overcome this limitation, we used a non-regularized two-dimensional sub-pixel correlation algorithm to estimate the relative horizontal offset between the pre- and post- 2010 El Mayor – Cucapah earthquake LiDAR acquisitions. This analysis shows an unbiased view of the vertical slip component of the rupture induced by the Mw 7.2 2010 El Mayor – Cucapah earthquake (Figure 2).

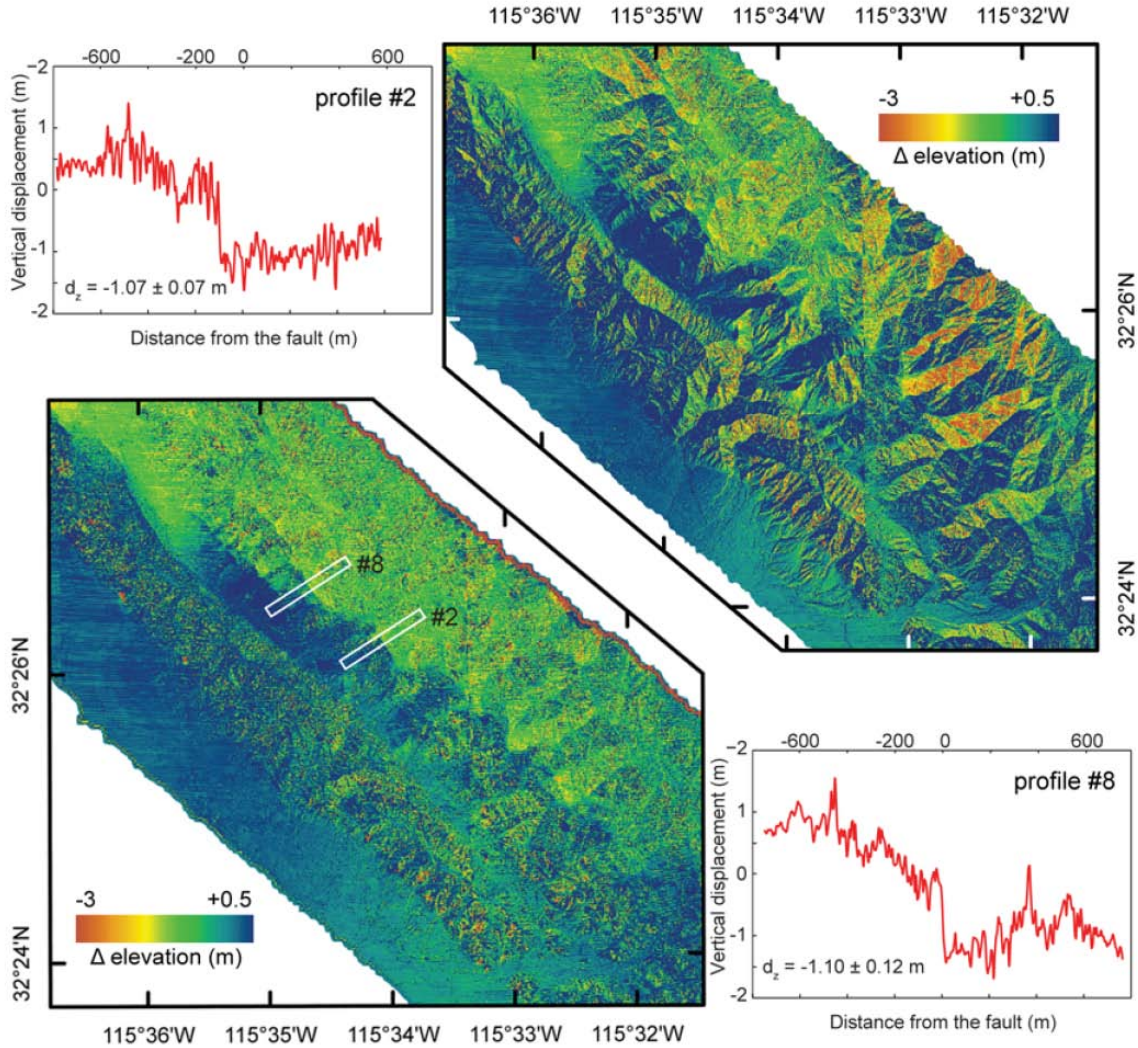

Figure 2. Pre and post earthquake LiDAR difference around the Puerta Accomodation zone. Top-right: before 2D image matching correction. The fault rupture cannot be seen and signal is overwhelmed by topographic artifacts. Lower-left: Pre and post-earthquake LiDAR difference once 2D image matching is applied to compensate for lateral offsets. The en-echelon pattern is clearly visible and surface rupture can be quantified from the corresponding profiles (upper-left and lower-right).

The previous examples show how 2D image matching can be applied to recover surface ruptures induced by large earthquakes using time-series of remote sensing data. However, one drawback of the previous technique is that it only relies on 2D image matching where the horizontal

component of the deformation is first deduced, and then the vertical component is derived by subtraction of the data shifted by the horizontal deformation. It therefore assumes that the deformation to be measured has separable horizontal and vertical components. Ideally, we are seeking an algorithm that can produce true 3D matching of topographic surfaces. Another strong limitation of the above example is that applying non-regularized image matching to recover the horizontal component of the deformation fails in areas of smooth or noisy topography, making it a technique that can only be applied opportunistically. For instance, when this technique was applied to smooth topography data such as over sand dunes surfaces, the motion of sand dunes could not be recovered (Figure 2).

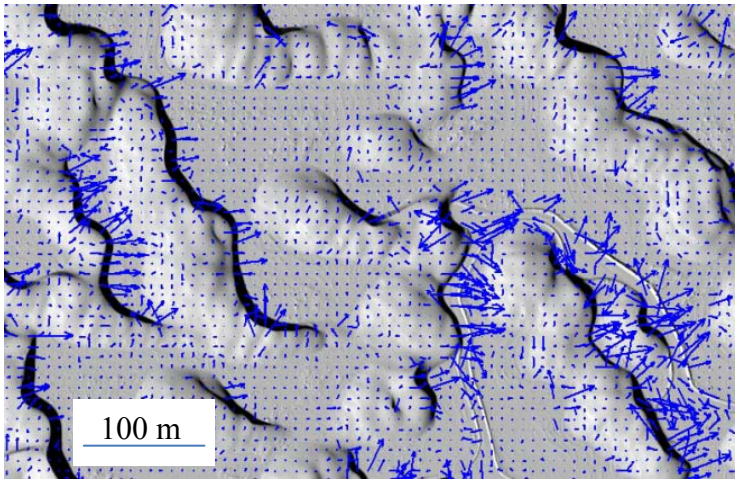

Figure 3: Horizontal offset map obtained from 2-D correlation of LiDAR DEM from the White Sand Dunes acquired in 2009 and 2010 [Ewing and Kocurek, 2010; Jerolmack et al., 2012; Reitz et al., 2010]. The correlation fails due to the smoothness of the dunes and produces noisy results near the dunes crests, which exhibits high contrast. A new matching technique is required to densely pair smooth 3D surfaces

This example highlights the difficulty of reliably retrieving the horizontal motion on smooth surfaces using standard correlation techniques.

We therefore set our efforts to derive an original 1D-2D-3D regularized image matching framework, which could be versatile enough to extract topography using 1D matching of stereo imagery (if we assume matching along epipolar lines), but also produce horizontal offset fields from 2D matching of passive optical data, and also delivers a rigorous 3D matching of DEM surfaces. We developed a single framework for these three tasks, which is possible if we consider that topography acquisitions (e.g., LiDAR point cloud) can be carefully transformed into images where the intensity defines the height. Hence, we addressed all three matching problems in a single image-matching framework. The advantages are two-folds: we design only one algorithm to solve three different problems, and we take advantage of the regular structure of pixels to speed up computation.

Image matching frameworks can be divided into two main categories: Heuristics driven methods and Optimization driven methods.

Heuristics methods rely on individually matching each point of the reference image. This matching can either be: (1) Sparse, a few points with strong features are matched, while the others are matched through a diffusion process that propagates the matching [23]; (2) Dense, all points are matched by finding the most probable correspondent in a search area, and then the results are filtered to remove outliers [13]. Heuristics methods are known to be sensitive to noise and outliers. They sometimes dramatically fail because of that.

Optimization driven methods transform the matching problem into a functional to minimize. This functional encodes: (1) a similarity term that locally forces the solution to be a tight matching, (2) a regularization term that enforces some user-defined properties of the solution such as smoothness or consistency with some physics-based properties. These methods are named global matching methods [12] as they process the problem globally, but they are generally too slow and too complex to be used with large images such as produced by remotely sensed instruments. Hence, for large images, the functional is typically decomposed into a set of smaller functionals that are optimized independently, to the detriment of quality. These last methods are referred to as semi-global matching methods and they represent the state of the art in satellite and aerial stereo-imaging [14].

Despite their promising performances, optimization driven methods exhibit two significant drawbacks: the functional is usually arbitrarily designed and the two terms, similarity and regularization, can be expressed in different metric space, and the optimization process is difficult as the functional is often non-linear and non-convex. We found that the functional can be derived from a probability leading to a mathematically sound metric space, and that the state of the art discrete optimization solvers can be employed to achieve reasonable computational time while using a true global matching formulation.

Given reference and target images, we want to find the most ***probable*** matching. This naturally lead us to work within the Bayesian framework. With no loss of generality we can relate probabilities to energies thanks to the Gibbs measure, and ensure that the functional lives in a well defined metric space. Our functional is sound to optimize, but it is still non linear and non convex. Hence, we slightly approximate our problem by discretizing the space of possible matches to optimize a discrete *Markov Random Field*. While this problem remains NP-Hard, it can be efficiently addressed with state of the art solvers. Particularly, we use the fastest solver available [15] based on the primal-dual scheme [16].

We produced two main contributions where we detail this new framework. These contributions only used 1D matching (image matching long epiplar lines) to introduce the framework in its most simple version:

1- In this first publication, we defined a global matching framework based on energy pyramid, the Global Matching via Energy Pyramid (GM-EP) algorithm, which estimates the disparity map by globally optimizing a coarse to fine sequence of sparse Conditional Random Fields (CRF) directly defined on the energy. This global discrete optimization approach guarantees that at each scale we obtain a near optimal solution, and we demonstrate its superiority over state of the art image pyramid approaches through application to real stereo-pairs. We conclude that multiscale approaches should be build on energy pyramids rather than on the traditional image pyramids.

   B.Conejo, S. Leprince, F. Ayoub, and J.P Avouac “Fast Global Stereo Matching via Energy Pyramid Minimization”, Photogrammetric Computer Vision Symposium - PCV2014, 2014.

2- In this second publication, we proposed a framework that significantly speeds-up graphical model optimization while maintaining an excellent solution accuracy. The proposed approach relies on a multi-scale pruning scheme that is able to progressively reduce the solution space by use of a strategy based on a coarse-to-fine cascade of learnt classifiers. Our framework constantly yields a significant time speed-up (with respect to the most efficient inference methods) and obtains a more accurate solution than directly optimizing the MRF.

   B.Conejo, N. Komodakis, S. Leprince, and J.P Avouac. Speeding-up Graphical Model Optimization via a Coarse-to-fine Cascade of Pruning Classifiers. Advances in Neural Information Processing Systems 27, 2014.

Thus far, we have mostly focused on deriving the theoretical framework, and in the publications our benchmarks focused on urban scenes because these are typically the most challenging cases with the highest discontinuities in topography around buildings. It's also usually in urban areas that ground truths are easier to find. Future work will focus on deriving 3D models for natural scenes, and the same framework will be used.

To prove that the extension of the framework to 3D topography matching indeed performs as expected, we also reconducted the failed experiment from Figure 3 (see Figure 4). We see that the global regularization of the algorithm allows it to behave as expected.

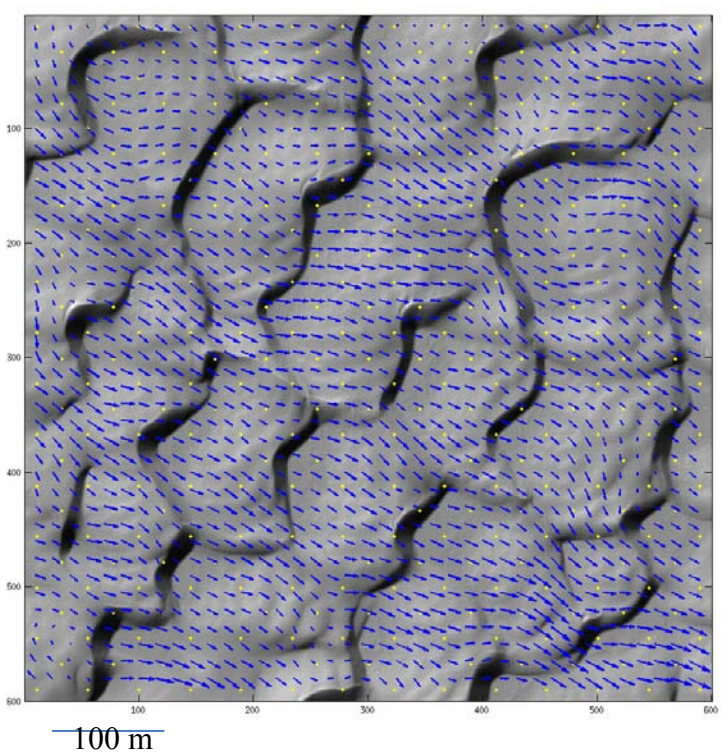

Figure 4: Dunes migration recovered from 2009-2010 LiDAR acquisition using our MRF framework. The framework minimizes a matching energy between LiDAR point clouds over patches defined by the network of control points (yellow dots). Although not yet validated, this early result shows the potential of our framework to the comparison of LiDAR data. The comparison with correlation methods is striking (Figure 2). The direction and magnitude of the recovered deformation seem consistent with visual inspection

We show two other applications of the framework using 3D matching of surfaces to look at both volume change, and 3D displacements. This work was presented at the AGU meeting fall 2013:

B.Conejo, S. Leprince, F. Ayoub, and J.P Avouac "A 2D and 3D registration framework for remote-sensing data," Abstract G33A-0971 presented at 2013, Fall Meeting, AGU, San Francisco, CA, 9-13 December..

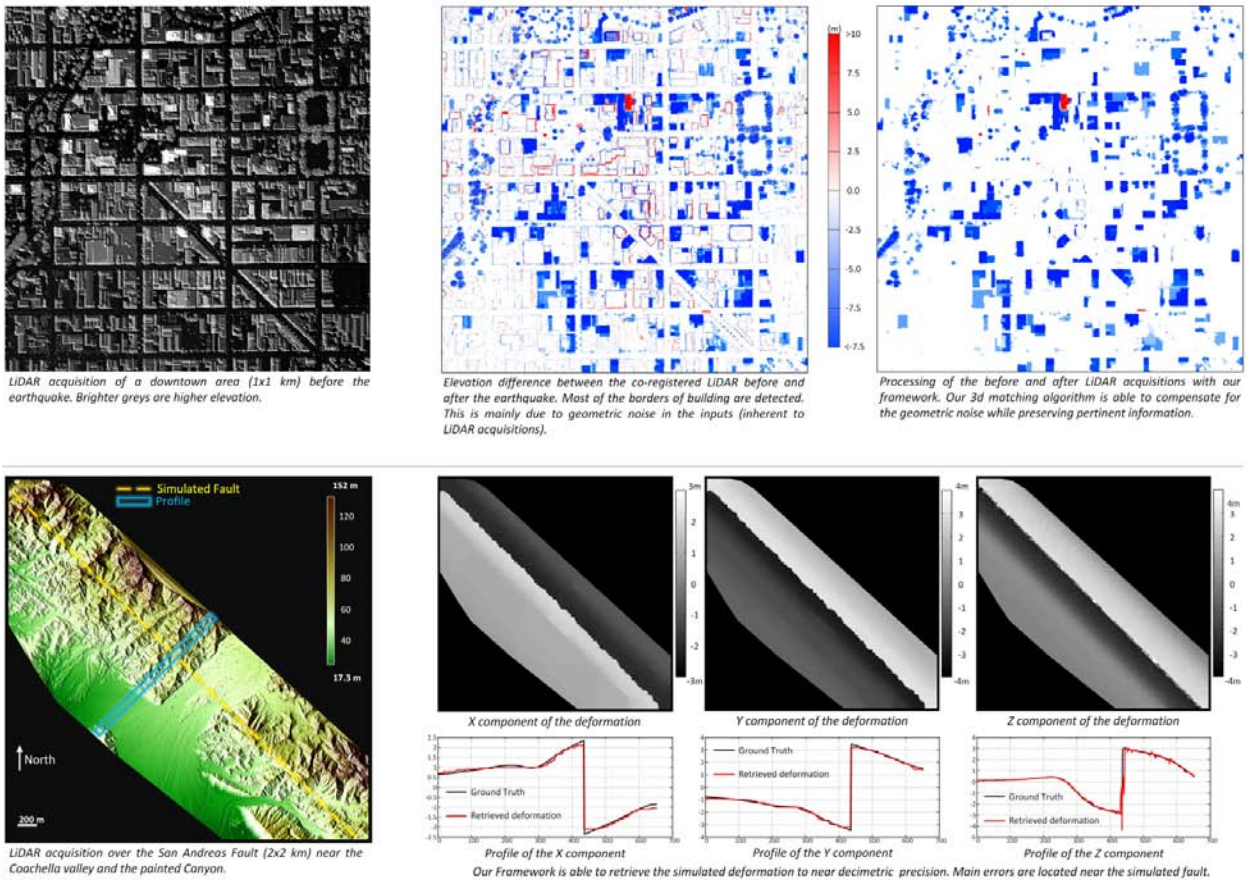

Figure 5: **(Top row)** The matching framework was used to compare changes between two urban Lidar acquired above the city of Christchurch before and after the 2011 earthquake that produced damages to buildings. Differencing the LiDAR bring out many artifacts, in particular at the edges of the building, where the LiDAR data may not align very well, or might be noisy due to shadowing. After applying the 3D matching framework and solving for local displacement of each LiDAR point in x,y,z, the z component represents the regularized elevation change and is robust against detection errors. **(Bottom row)** We simulated an earthquake using a simple Okada dislocation model and applied it to a piece of LiDAR from the USGS B4 data. The 3D matching was able to nicely recover the deformation field applied in the three dimensions with good accuracy despite the L1 norm gradient regularization of the algorithm.

CONCLUSION AND FUTURE WORK

We developed a new framework that is versatile enough to accommodate 1D, 2D, and 3D image matching. We put the emphasis on quality of matching, versatility of data, and computational speed. Although we report in the publications ways to speed up the computation by up to 80%, the complexity of the algorithm still makes it hard to apply to large high dimensional problems, such as 3D LiDAR matching. Further efforts are needed to gain further computational speed increase. Nevertheless, we have opened new ways to quantitatively exploit a wide variety of remote sensing data and further work will include the proposed algorithm in the COSI-Corr toolbox released on the Caltech website[1].

CITATIONS

[1] http://www.tectonics.caltech.edu/slip_history/spot_coseis/index.html
[2] http://browse.digitalglobe.com/imagefinder/main.jsp.
[3] http://www.opentopography.org/
[4] Hugenholtz, C. H., N. Levin, T. E. Barchyn, and M. C. Baddock (2012), Remote sensing and spatial analysis of aeolian sand dunes: A review and outlook, Earth-Science Reviews, 111(3-4), 319-334.
[5] Leprince, S., E. Berthier, F. Ayoub, C. Delacourt, and J. P. Avouac (2008), Monitoring Earth Surface Dynamics with Optical Imagery, EOS, Transactions, American Geophysical Union, 89(1).
[6] Avouac, J. P., F. Ayoub, S. Leprince, O. Konca, and D. V. Helmberger (2006), The 2005, M-w 7.6 Kashmir earthquake: Sub-pixel correlation of ASTER images and seismic waveforms analysis, Earth and Planetary Science Letters, 249(3-4), 514-528.
[7] Ayoub, F., S. Leprince, and J. P. Avouac (2009), Co-registration and correlation of aerial photographs for ground deformation measurements, Isprs Journal of Photogrammetry and Remote Sensing, 64(6), 551-560.
[8] Leprince, S., S. Barbot, F. Ayoub, and J. P. Avouac (2007), Automatic and precise orthorectification, coregistration, and subpixel correlation of satellite images, application to ground deformation measurements, Ieee Transactions on Geoscience and Remote Sensing, 45(6), 1529-1558.
[9] Van Puymbroeck, N., R. Michel, R. Binet, J. P. Avouac, and J. Taboury (2000), Measuring earthquakes from optical satellite images, Applied Optics, 39(20), 3486-3494.
[10] A. Trouvé and L. Younes. (2011) "Shape Spaces" in Handbook of Mathematical Imaging, p 1309--1362. Springer,.
[11] Haker, S., L. Zhu, A. Tannenbaum , S. Angenent, (2004), Optimal mass transport for registration and warping, International Journal on Computer Vision
[12] Kolmogorov, V. and R. Zabih (2005), Graph Cut Algorithms for Binocular Stereo with Occlusions, Mathematical Models in Computer Vision: The Handbook, Springer-Verlag,
[13] Monasse, P and P. Tan Stereo Disparity through Cost Aggregation with Guided Filter (2013), IPOL pre-print
[14] http://www.micmac.ign.fr/
[15] Kappes, J., N. Komodakis and Al, A Comparative Study of Modern Inference Techniques for Discrete Energy Minimization Problems (2013), Oral presentation CVPR.
[16] Komodakis, N., G. Tziritas and N. Paragios (2007), Fast, Approximately Optimal Solutions for Single and Dynamic MRFs, technical report CVPR.

[17] Komodakis, N. (2010), Towards More Efficient and Effective LP-based Algorithms for MRF Optimization, ECCV 2010
[18] Komodakis, N. (2011), Learning to Cluster Using High Order Graphical Models with Latent Variables, ICCV 2011
[19] Chan, T. F., B. Sandberg, and L. A. Vese (2012), Active Contours Without Edges for Vector-Valued Images, Journal of Visual Communication and Image Representation, 11, 130-141.
[20] http://www.ipol.im/pub/pre/H1/
[21] Brown, L. G. (1992), A Survey of Image Registration Techniques, ACM Computing Surveys
[22] Zitova, B. and J. Flusser (2003), Image registration methods: a survey, Image and Vision Computing, Vol. 21, ELSEVIER
[23] Goshtasby, A. A. (2005), Image registration for medical, remote sensing and industrial applications. WILEY